



ELSEVIER

Contents lists available at ScienceDirect

Planetary and Space Science

journal homepage: www.elsevier.com/locate/pss

Magnetic field modulated dust streams from Jupiter in interplanetary space

Alberto Flandes^{a,*}, Harald Krüger^{b,c}, Douglas P. Hamilton^d, J. Francisco Valdés-Galicia^a, Linda Spilker^e, Rogelio Caballero^a^a Ciencias Espaciales Instituto de Geofísica, UNAM, Ciudad Universitaria, Coyoacán 04510, México D.F., Mexico^b Max-Planck-Institut für Sonnensystemforschung, 37191 Katlenburg-Lindau, Germany^c Max-Planck-Institut für Kernphysik, 69029 Heidelberg, Germany^d University of Maryland, College Park, MD 20742-2421, USA^e Jet Propulsion Laboratory/California Institute of Technology, Pasadena, USA

ARTICLE INFO

Article history:

Received 27 October 2010

Received in revised form

24 May 2011

Accepted 25 May 2011

Available online 16 June 2011

Keywords:

Interplanetary dust

Solar wind

Jupiter

Io

ABSTRACT

High speed *dust streams* emanating from near Jupiter were first discovered by the Ulysses spacecraft in 1992. Since then the phenomenon has been re-observed by Galileo in 1995, Cassini in 2000, and Ulysses in 2004. The dust grains are expected to be charged to a potential of ~ 5 V, which is sufficient to allow the planet's magnetic field to accelerate them away from the planet, where they are subsequently influenced by the interplanetary magnetic field (IMF). A similar phenomenon was observed near Saturn by Cassini. Here, we report and analyze simultaneous dust, IMF and solar wind data for all dust streams from the two Ulysses Jupiter flybys. We find that compression regions (CRs) in the IMF – regions of enhanced magnetic field – precede most dust streams. Furthermore, the duration of a dust stream is roughly comparable with that of the precedent CR, and the occurrence of a dust stream and the occurrence of the previous CR are separated by a time interval that depends on the distance to Jupiter. The intensity of the dust streams and their precedent CRs are also correlated, but this correlation is only evident at distances from the planet no greater than 2 AU. Combining these observations, we argue that CRs strongly affect dust streams, probably by deflecting dust grain trajectories, so that they can reach the spacecraft and be detected by its dust sensor.

© 2011 Elsevier Ltd. All rights reserved.

1. Introduction

The spectacular volcanic plumes of Jupiter's moon Io inject copious amounts of gas and fine dust along Io's orbit, leading to the so-called Io plasma torus at $\sim 5.9R_J$ distance from Jupiter (Jupiter radius $R_J = 71,492$ km). Dust grains in Io's volcanic plumes get easily charged in Io's ionosphere (Flandes, 2004) and transported into the plasma torus (Horányi et al., 1993). At least 1 kg of sub-micrometric (~ 10 nm) dust grains escape every second from the torus to the circum-Jovian space (Krüger et al., 2003). Due to their electric charge and small size, their motion is dominated by electromagnetic forces. It has been demonstrated that the induced corotating electric field of the huge Jovian magnetic field accelerates positively charged grains away from Jupiter. The grains get sufficiently large speeds (≥ 200 km s^{-1}) that they can easily escape from the magnetosphere (Horányi et al., 1993; Hamilton and Burns, 1993).

This escape was first observed by Ulysses in 1992 and confirmed by the Galileo (1995) and Cassini (2000) spacecraft which detected this dust outside the Jovian magnetosphere as a discontinuous, but periodic flux coupled to the interplanetary magnetic field (IMF) (Grün et al., 1993, 1998; Flandes and Krüger, 2007). This phenomenon was called the Jovian dust streams. The Cassini spacecraft detected dust streams escaping from the Saturn system as well in 2004 (Kempf et al., 2005a). It was shown that these two phenomena shared similar properties. The saturnian dust streams source is not well defined yet, however, the cryovolcanic jets from the south pole of the Moon Enceladus appear to be good candidates (Jones et al., 2009). Nevertheless, the saturnian charged dust grains also escape via the corotational electric field of Saturn mainly along the planet's equatorial plane (Kempf et al., 2005b; Maravilla and Flandes, 2005). Recently Hsu et al. (2010) explained the saturnian dust stream detection by Cassini CDA (Cosmic Dust Analyzer) in connection to the IMF and concluded that the saturnian dust streams particles were directly correlated to the sector structure of the IMF, in particular the positive sectors.

In this work we concentrate on the Jovian dust streams detected during the two flybys of the Ulysses spacecraft at Jupiter (1991–1992 and 2003–2005). This data set is, by far, the most

* Corresponding author. Tel.: +52 55 5622 4113.

E-mail addresses: flandes@geofisica.unam.mx, aflandes@jpl.nasa.gov (A. Flandes).

complete and comprehensive presently available (Krüger et al., 2010). We present the full data set in a series of 13 plots (Fig. 1a–m) that will be discussed throughout this work. Our intention is to give the reader a better understanding of the detection and analysis of dust streams, and to elucidate the close connection that they have with the IMF and the solar wind. We investigate the significance of Corotating Interaction Regions (CIRs) and Coronal Mass Ejections (CMEs) for the formation of the Jovian dust streams in interplanetary space. A very first approach to this study was sketched in Flandes and Krüger (2007), nevertheless in this work we present a more thorough and extensive analysis.

2. The Ulysses trajectory and the Jovian dust

The Ulysses spacecraft was launched toward Jupiter in October 1990. In early 1992, during the first Jupiter flyby, a swing-by manoeuvre changed the inclination of its orbit to 79° with respect to the ecliptic plane. Since then, Ulysses has been on an eccentric heliocentric trajectory with an approximately six-year period and 5.4 AU aphelion distance. Ulysses is no longer active. After almost 19 years and a very successful mission, the Ulysses spacecraft was switched off in June 2009. Fig. 2 shows the orbits of Jupiter and Ulysses about the Sun during the second Jupiter flyby. The two Ulysses flybys differed in geometry as can be seen in the top panels of Fig. 3a and b that show the profiles of the Ulysses angular position with respect to Jupiter.

During the first flyby, Ulysses approached Jupiter to $6.3R_J$ moving close to the ecliptic plane and close to the Jupiter–Sun

line (Fig. 3a, top panel), i.e. at low jovigraphic and ecliptic latitudes and low jovigraphic longitudes. After flyby, Ulysses moved away from the planet at approximately -35° jovigraphic latitude.

During the first flyby, Ulysses scanned only a narrow region of circum-Jovian space, but its radial distance was very close to Jupiter ($6.3R_J$). During the second flyby, between 2002 and 2004 (Fig. 3b, bottom panel), the spacecraft scanned a wider range of jovigraphic latitudes and longitudes: Ulysses sampled more than 120° in longitude and more than 100° in latitude. During this second flyby, Ulysses approached Jupiter to only 0.8 AU in early 2004.

2.1. Dust stream detection and identification

Ulysses detected the very first dust stream as a weak burst in late September 1991, at $r=1.1$ AU distance from Jupiter while heading toward Jupiter along the ecliptic plane at a jovigraphic longitude of $L \approx 11^\circ$. Jovigraphic longitudes are defined with respect to the Sun–Jupiter–spacecraft angle. The Jupiter–Sun vector defines $L=0^\circ$. Positive longitudes correspond to angles to the left of that imaginary line (in the direction of Jupiter’s motion)—see Fig. 2. We also define the jovigraphic latitude, β , as the angle measured with respect to the Jovian equatorial plane. Positive latitudes correspond to the northern hemisphere and negative latitudes to the southern hemisphere. We ignore the small tilt of Jupiter’s rotation axis (1.31°) and that of the solar equator (6.09°) and assume that these are coplanar.

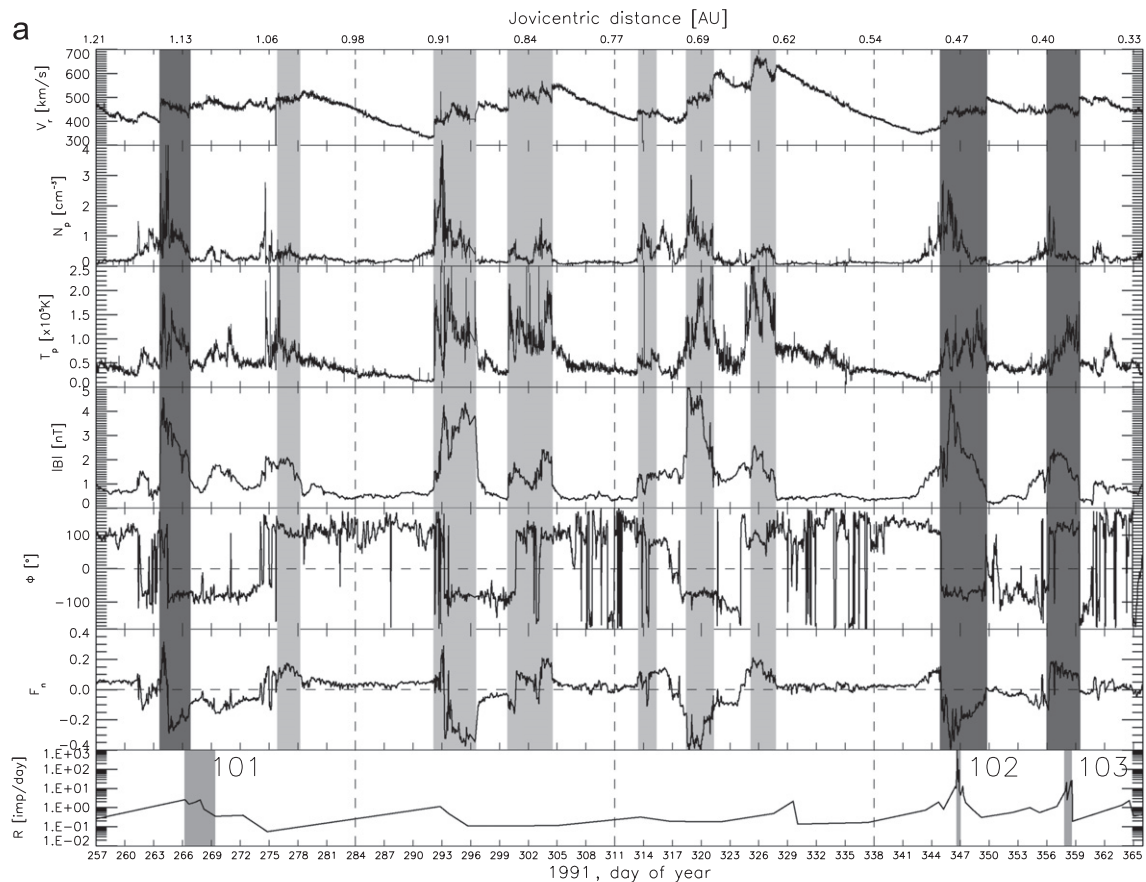


Fig. 1. (a)–(m) Ulysses solar wind, interplanetary magnetic field and dust data from both Jupiter flybys: solar wind speed V , proton density N_p , proton maximum temperature T_p , IMF intensity $|B|$ and azimuthal angle Φ . Next is the vertical Lorentz force F_e in arbitrary units and finally the dust impact rate. Data is organized in multiple integers of solar rotation periods (~ 27 days) to highlight periodicities. The dark gray numbered bars in the bottom panel indicate the dust stream peaks in every case. The gray stripes indicate compression regions. The darker stripes indicate those events that precede and are associated to dust streams. Fig. 1b shows a gap in the data series between days 33 and 46. Jovicentric distance is shown at the top.

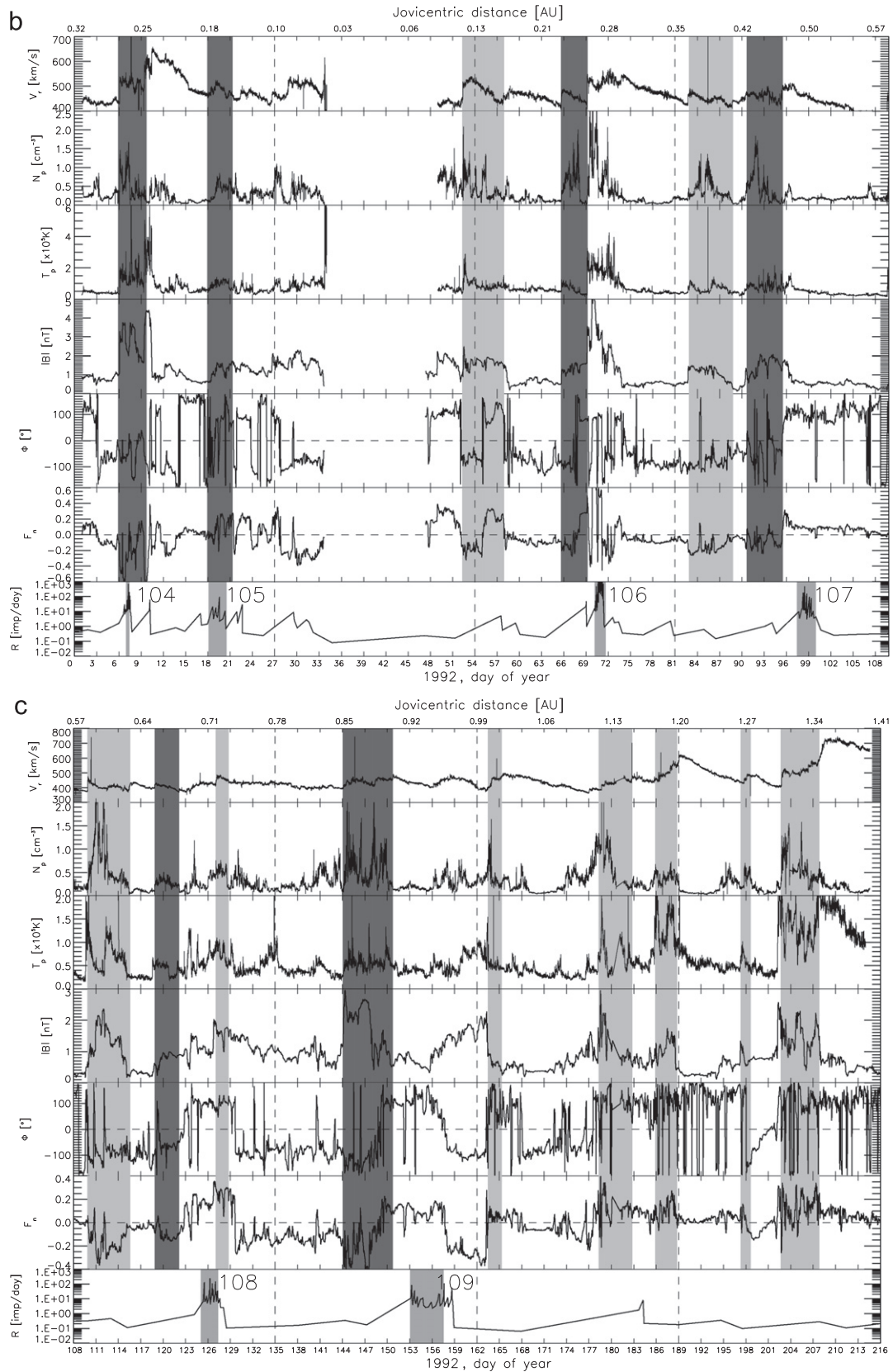


Fig. 1. (continued)

During this first flyby, 11 dust streams were detected, five before the closest approach and six while the spacecraft was flying away from Jupiter. The last dust stream of this flyby was detected on 19 October, 1992 about 2 AU away from Jupiter.

During the second flyby, the first dust stream was detected in November 2002 as a weak burst as well, but this time, when the spacecraft was at $r=3.4$ AU, three times farther away from Jupiter as compared to the first dust stream from the first flyby. Then the

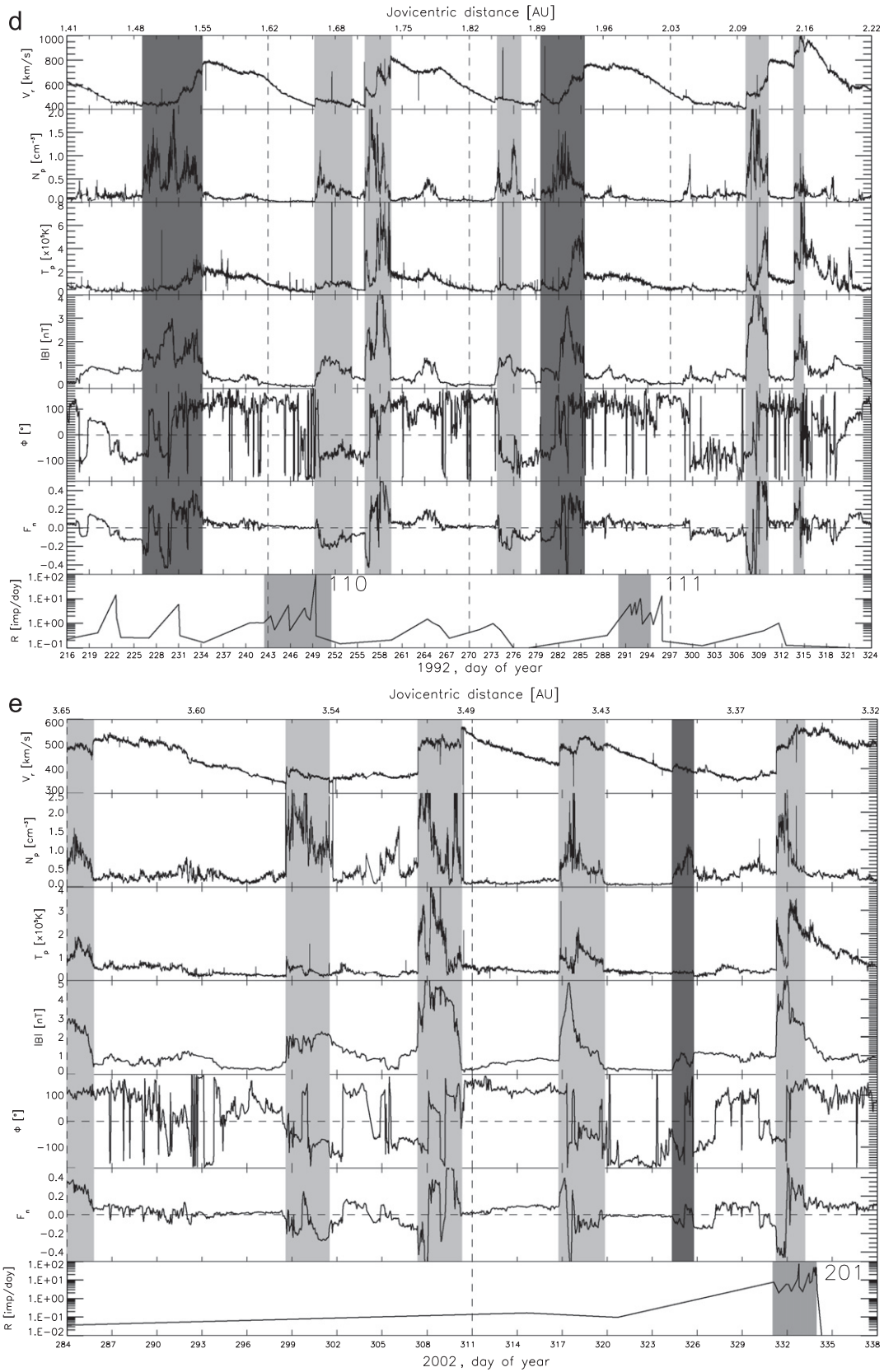


Fig. 1. (continued)

spacecraft was at a jovigraphic longitude and latitude $L = -37^\circ$ and $\beta = 44^\circ$. Unfortunately, after the detection of this dust stream the dust detector was switched off on 1st of December of 2002 for

a 6 month period for power saving reasons on board the spacecraft. Nevertheless many more streams were observed when the detector was switched on again on 3 June 2003. The data indicate

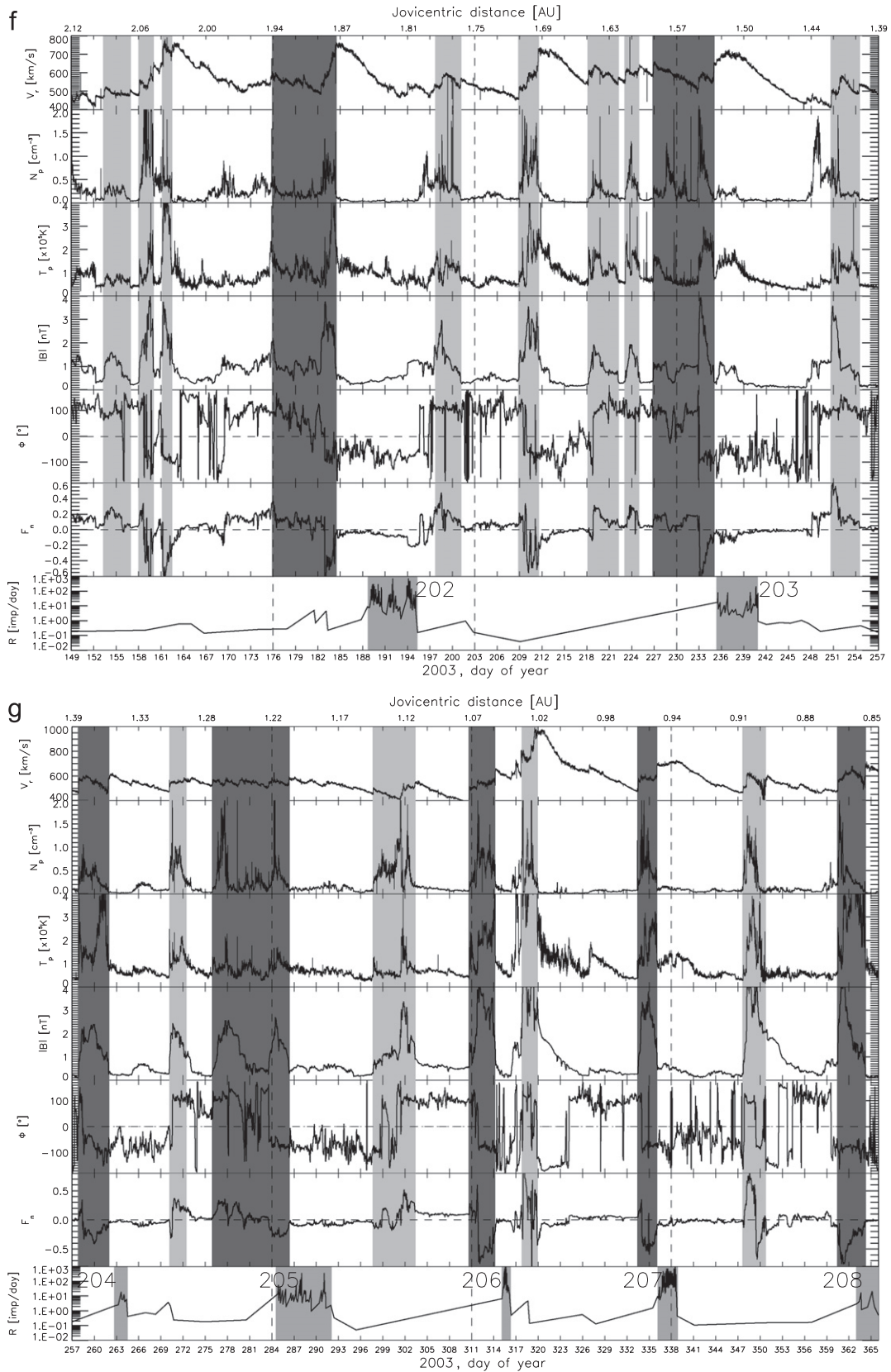


Fig. 1. (continued)

that dust streams are detected fairly uniformly in a wide range of jovigraphic latitudes and longitudes. In total, 28 dust streams were registered, nine before the closest approach and 19 while Ulysses was receding in radial distance from the planet. Actually

the last dust stream was detected on 16 August 2005 around 4 AU away from Jupiter (Krüger et al., 2006b).

The earliest dust stream identification was made by Grün et al. (1993) and the streams have been a topic of intense study for over

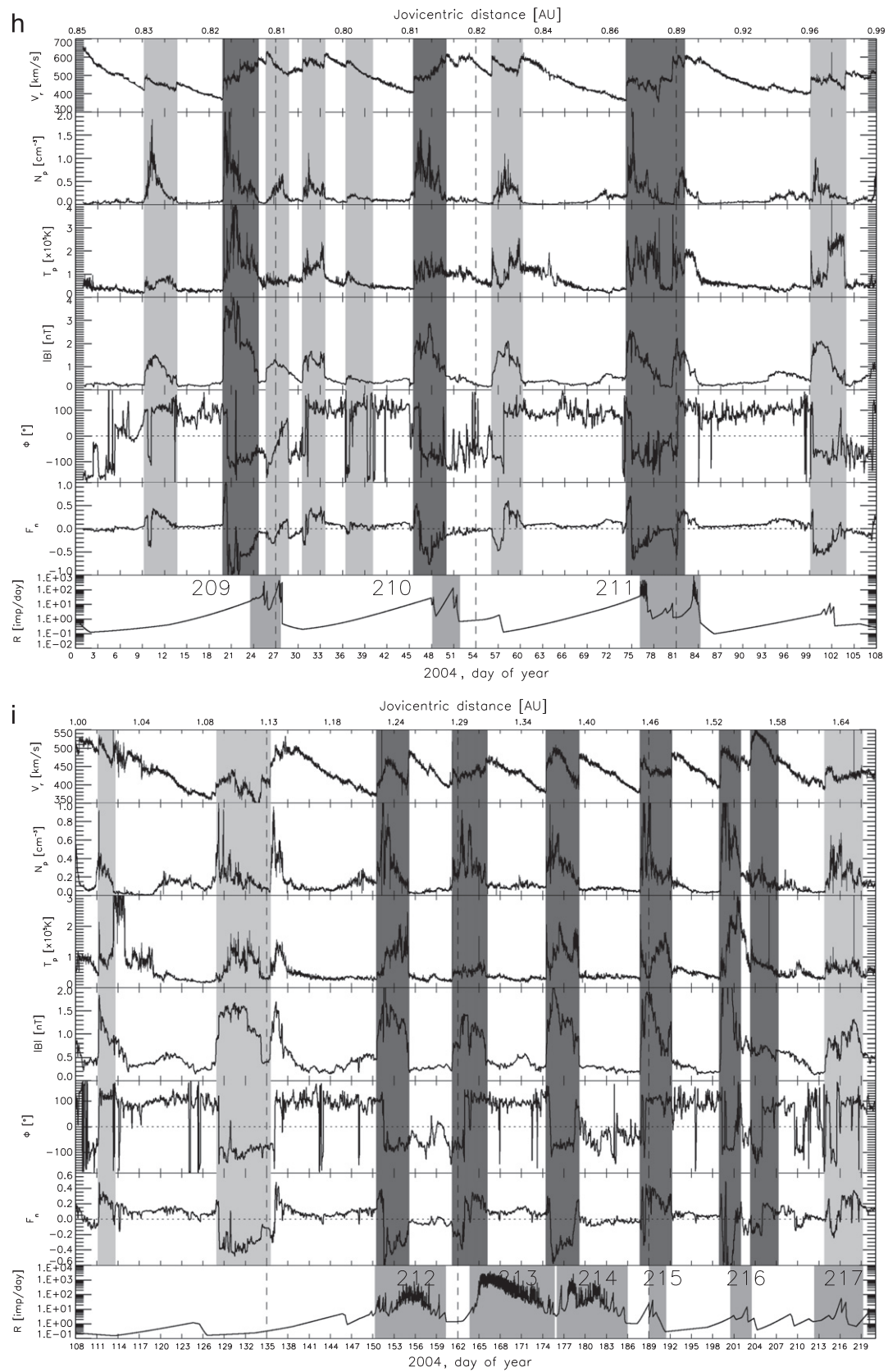


Fig. 1. (continued)

15 years. In all cases, dust streams were identified with probabilistic methods based on Poisson statistics (Oberst and Nakamura, 1991). This method separates true dust streams from chance

random fluctuations in the dust impact rate. In our work, we adopt the dust stream identifications and other relevant parameters from Baguhl et al. (1993) and Krüger et al. (2006b).

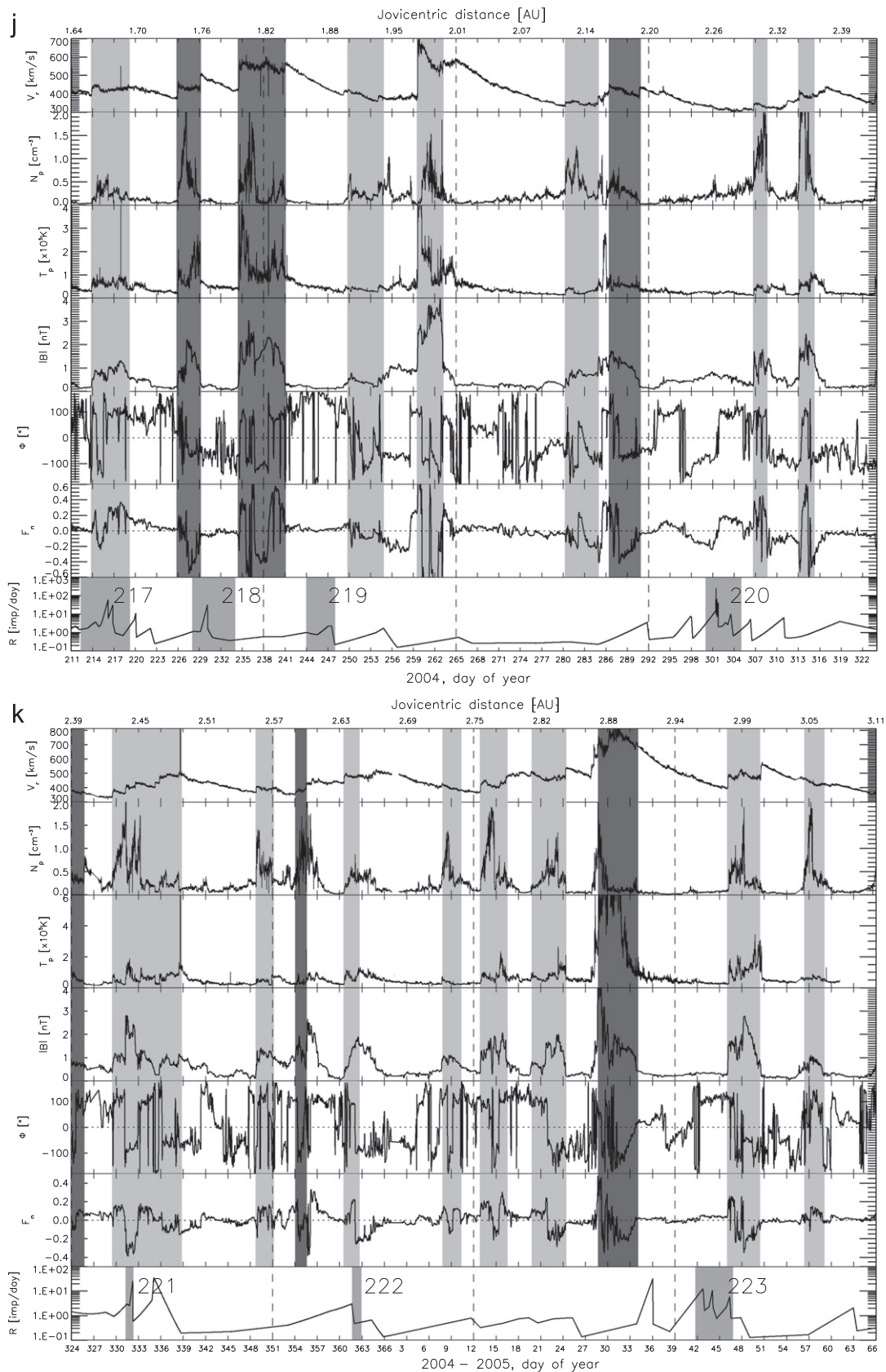


Fig. 1. (continued)

The first work provides a description of the Ulysses first flyby dust stream identification and the second work provides a comprehensive up-to-date summary of all the Ulysses dust streams from

the second flyby. We keep the stream numbers and order after Baguhl et al. (1993) and Krüger et al. (2006b), but for practical purposes, we will designate the streams of the first flyby as

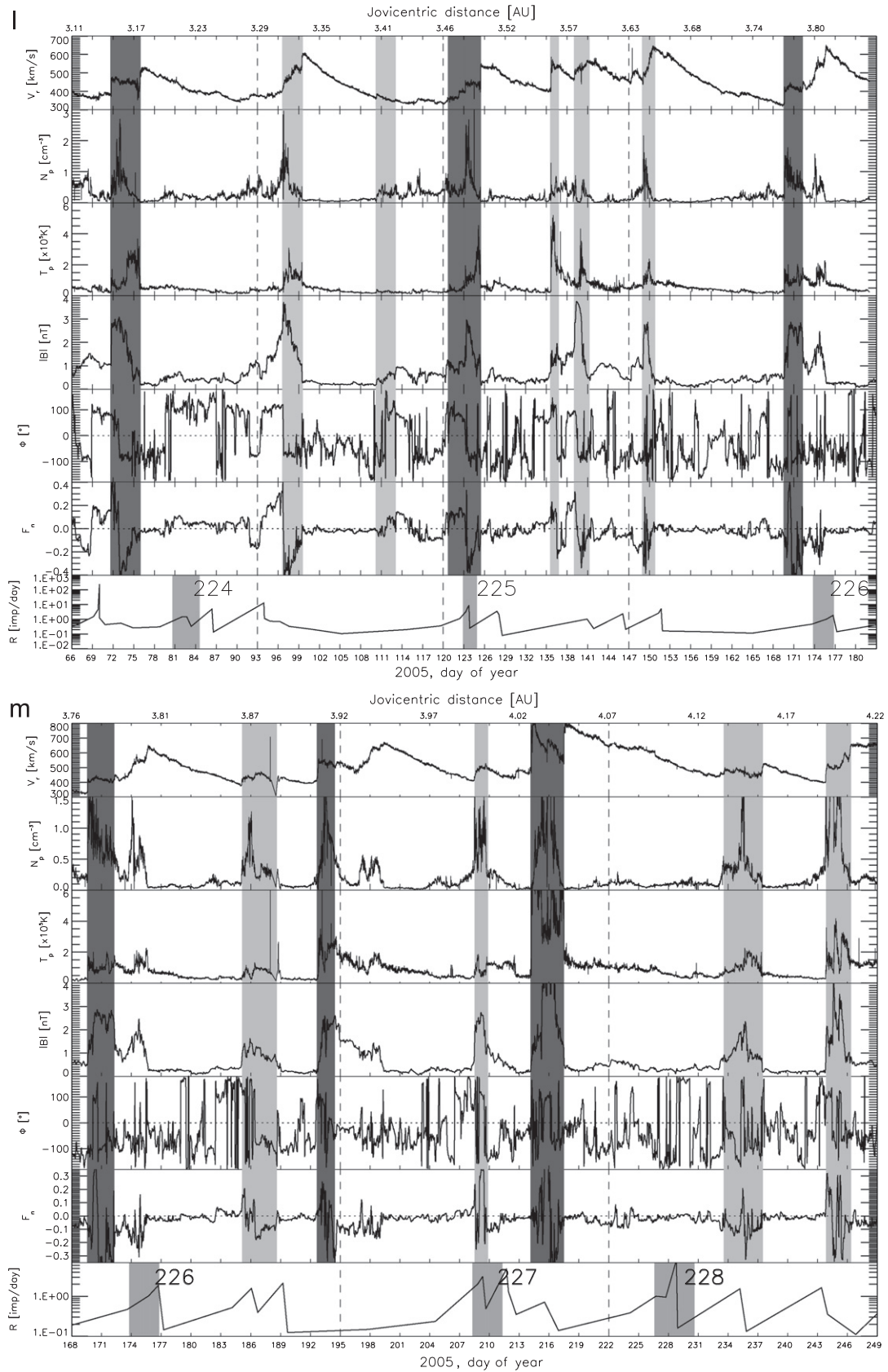


Fig. 1. (continued)

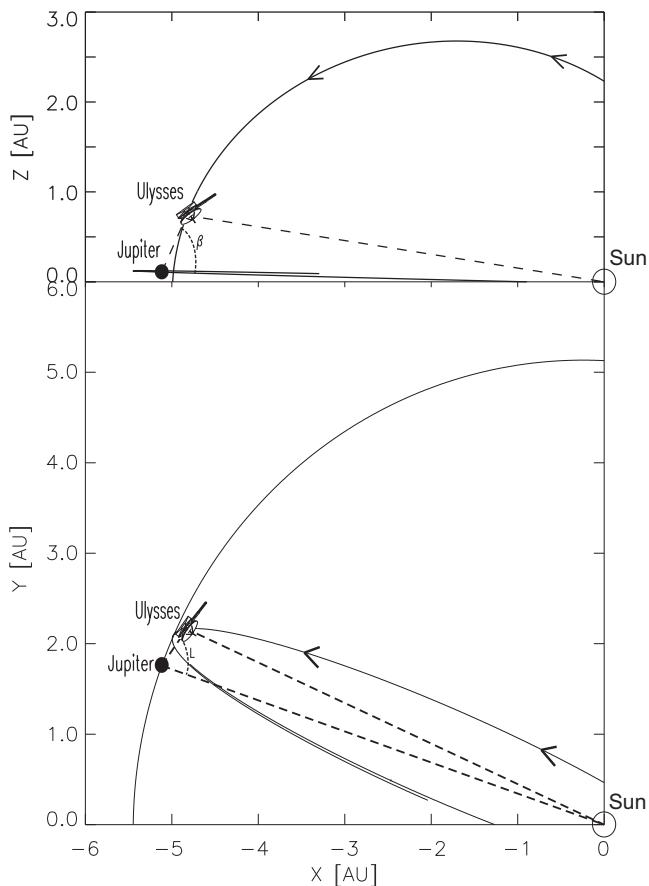


Fig. 2. Projection of the orbit of the Ulysses spacecraft on the XZ plane (top panel) and the XY plane (ecliptic plane, bottom) during the second Jupiter flyby. The positions of Ulysses and Jupiter at their closest approach (5 February 2004, distance $r = 0.8$ AU) are indicated. Jupiter defines the origin of this coordinate system. β and L represent the jovigraphic latitude and longitude angles with the Jupiter–Sun direction as their starting measuring position or zero. At the shown positions $\beta = +54.1^\circ$ and $L = +73.4^\circ$.

streams 101 through 111 and those of the second flyby as 201 through 228, where the first digit stands for the flyby number and the last two for the dust stream number (see Table 1 and bottom panel of Fig. 1a–m).

3. The IMF, the solar wind and the dust streams

Grün et al. (1993) suggested that dust streams could be connected to Corotating Interaction Regions (CIRs). Hamilton and Burns (1993) proposed a model that explained the periodicity of dust streams through the successive and alternate deflections of the dust trajectories by the periodic change of polarity of the interplanetary magnetic field (IMF). In 2006, in the dust stream data set from the second Jupiter flyby, Krüger et al. (2006b) found correlations between the intensities of the radial (B_R) and tangential (B_T) magnetic field components and some of the dust streams' properties as well as footprints of the solar rotation period.

3.1. CIR and CME identification

The solar wind is a supersonic nearly radial outward flow of plasma that forms the heliosphere. It results from the expansion of the outermost layer of the Sun, the corona, and carries away the solar magnetic field, which is twisted due to the rotation of

the Sun. This leads to the structure known as the Archimedean spiral.

Observations (Krieger et al., 1973) have established that coronal holes at the Sun are stable sources of fast wind that lead to a pattern of corotating fast and slow solar wind flows in the heliosphere. The increasing interaction between these two flows with distance from the Sun generates the confined regions known as Corotating Interaction Regions, or CIRs, that evolve as corotating spirals in the solar equatorial plane. CIRs are bound by a forward pressure wave as leading edge that propagates into a slower moving plasma, and a reverse compression wave as trailing edge propagating back into a faster plasma. In contrast, Coronal Mass Ejections, or CMEs, are events where relatively dense and discretely bound coronal material are propelled outwards from the Sun to the interplanetary space.

For our analysis we use IMF and solar wind data obtained from the Ulysses spacecraft homepage (<http://ulysses.jpl.nasa.gov/>). The solar wind parameters (rows 1–3) are derived from the Swoops/Ion experiment (see Bame et al., 1992 for further details). These instruments measured the vector of the IMF and the speeds and densities of the solar wind plasma; while IMF parameters (rows 4 and 5 in Fig. 1) are derived from the VHM/FGM experiment (Vector Helium Magnetometer/Flux Gate Magnetometer experiment; we refer the reader to Balogh et al., 1992) for further details.

For CIR and CME identification purposes, in Fig. 1a–m, we plot the main properties of the solar wind and the IMF. These are the proton speed (V), number density (N_p) and temperature (T_p), as well as the intensity of the magnetic field vector B and the azimuthal angle of the magnetic field defined as Φ .

We assume that the proton species dominate the solar wind and their properties reflect well those of the bulk solar wind. We also consider that the dynamics of charged grains is mainly dominated by the tangential component of the magnetic field vector (see panel 4 of Fig. 1a–m). The latter assumption applies because at Jupiter, the IMF vector roughly lies in the ecliptic plane and it is also roughly perpendicular to the Jupiter–Sun line.

CIRs are a common and repetitive feature of the solar wind. They are bounded by shocks which cause sharp changes to the solar wind speed V at both their leading and trailing sides. A nice train of five CIRs associated with streams 212–216 can be seen in Fig. 1i, between days 150 and 203 in 2004—note the sharp vertical steps in V that bound the CIRs.

The first step is the fast forward shock produced when the fast solar wind plasma reaches and collides with the leading slow solar wind plasma, and the second step is the reverse shock produced when the rear fast wind tries to detach itself from the trailing slow wind. Additionally, we see well defined enhancements in B , T_p and N_p , all of which are expected when plasma is significantly compressed.

In summary, our method of CIR identification relies on the abrupt increase in the solar wind speed at the beginning correlated with strong enhancements of the magnetic field strength. The identification is confirmed with the simultaneous enhancement of the plasma number density and temperature. We state that whether we may be using a computer algorithm to identify the IMF enhancements, a second confirmation by direct inspection of the data, was always necessary.

Identification of CMEs follows slightly different rules. During a CME, we still expect enhancements of the IMF strength and solar wind parameters N_p and V . Although, the fastest and most evident CMEs show a leading shock (sharp change in V), they do not have a rear bounding shock. Instead, the plasma speed declines smoothly until it reaches average solar wind speed values. This is the main distinguishing characteristic between CIRs and CMEs. Additional clues come from the fact that CIRs are expected to

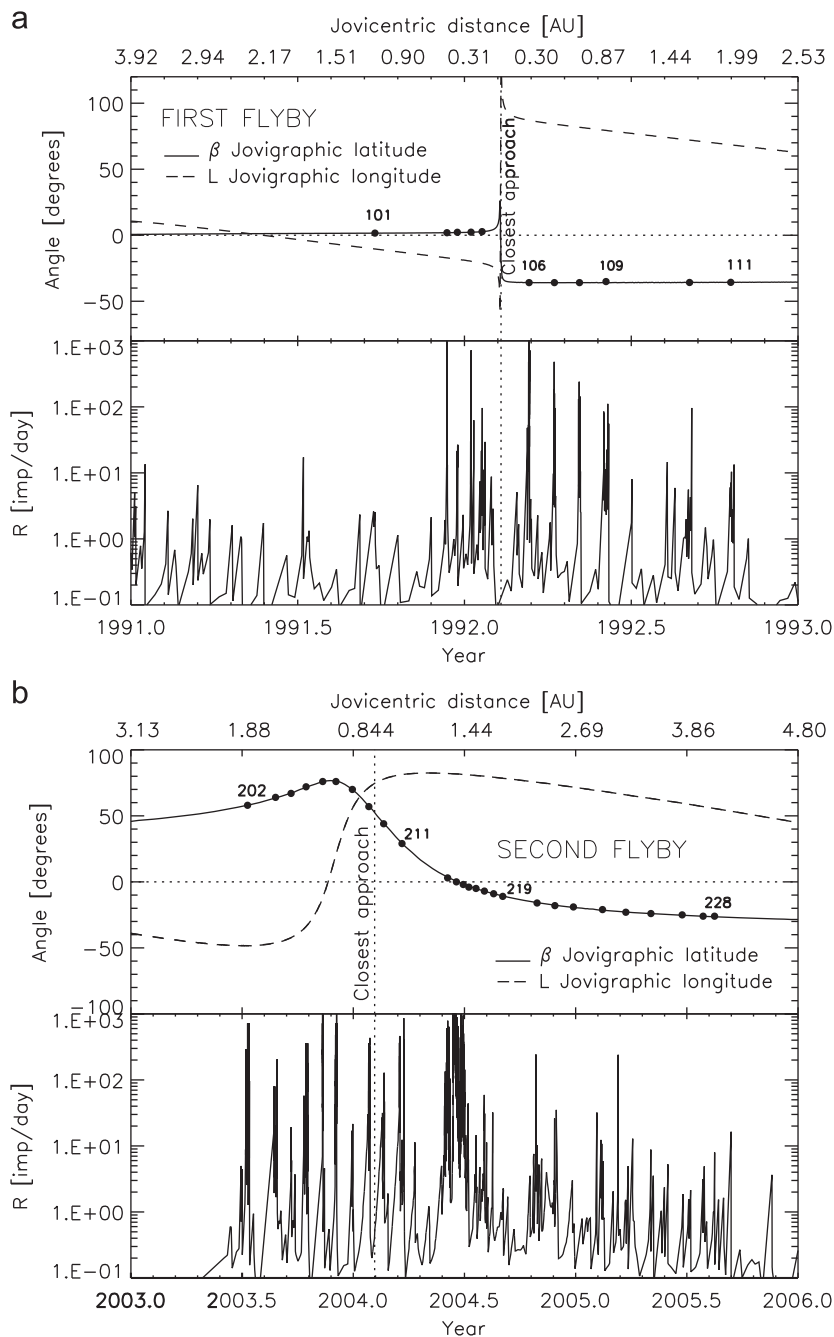


Fig. 3. Ulysses angular position with respect to Jupiter during the first (top) and second (bottom) Jupiter flybys (stream 201 is not included). The dust impact rate is displayed to highlight the dust flux variation with distance to Jupiter. The jovigraphic latitude, β , is measured with respect to the Jovian equatorial plane. Positive latitudes correspond to the northern hemisphere and negative latitudes to the southern hemisphere. Jovigraphic longitudes are measured with respect to the Jupiter–Sun line ($L=0^\circ$). Positive longitudes are measured in the counter-clockwise directions and vice versa (Fig. 2).

occur, on average, twice per solar rotation period (every two weeks) when the spacecraft crosses the Sun's current sheet, while CMEs show no periodicity and are greatly outnumbered by the CIRs. Finally, at Jupiter's distance CMEs are usually magnetically weak compared to CIRs. CMEs connected to dust streams are not very obvious in Fig. 1, but one intense example can be seen in Fig. 1j around day 259 in 2004. A clear single step in V is observed at the beginning of the event but there is no second step.

Both Ulysses flybys of Jupiter occurred shortly after solar maxima (1990–1991 and ~ 2001) so, in some cases, the solar wind appears quite perturbed. This makes the identification of the solar wind structures especially complex, leading to uncertainties in some cases. Despite these uncertainties, it is clear that most of

the 39 dust streams detected in both flybys are connected to CIRs rather than CMEs. From Ulysses' first pass by Jupiter, at most three of 11 dust streams (streams 105, 109 and 110) are likely related to CMEs. From the second flyby, five streams seem linked to one of these events (201, 202, 203, 217 and 225). Some identifications of solar wind events are uncertain. For example, it appears as if stream 201 is correlated with a CME that occurred began on day 324 (or perhaps 326), but which has an unclear-ending time. In addition, the events prior streams 202 and 203 seem to combinations of both CIRs and CMEs (Table 1).

In Table 1, we summarize all events connected to dust streams and mark some special cases with asterisks. Still, we highlight that our interest lies in the solar wind magnetic field enhanced

Table 1

Dust streams parameters and related high IMF events identified in the Ulysses data set: flyby/N: stream identification number (1); dust stream peak year and day (2); Δt_s : dust stream duration (3); r : joviocentric distance (4); β : jovigraphic latitude (5); L : jovigraphic longitude (6); Fr^2 : dust stream flux (7); EVENT: precedent CIR (normal text) or CME (italics) occurrence and duration (8); Δt_c : event duration (9); Δt : period between precedent event-peak and following dust stream peak (10); $|B|$: event maximum magnetic field intensity (11). Data in columns (1)–(5) and (7) were taken from Baguhl et al. (1993) and Krüger et al. (2006b).

Flyby/N (1)	Year/day (2)	Δt_s (days) (3)	r (AU) (4)	β (°) (5)	L (°) (6)	Fr^2 ($m^{-2}s^{-1}AU^2$) (7)	EVENT (year/days) (8)	Δt_c (days) (9)	Δt (days) (10)	$ B_{max} $ (nT) (11)
101	91/267.8	3.2	1.1	1.6	10.55	0.0109	91/263.7–266.7	3.1	2.5	4.55
102	91/346.8	0.4	0.5	1.9	17.28	0.0094	91/345.0–349.7	4.8	1.6	4.91
103	91/358.2	0.8	0.4	2.2	18.38	0.0017	91/356.1–359.4	3.4	1.8	2.45
104	92/007.2	0.4	0.3	2.3	19.79	0.0024	92/006.0–009.6	3.6	1.0	4.06
105	92/019.3	2.4	0.2	2.7	21.32	0.0010	92/018.0–021.3	3.2	0.1	1.70
106	92/070.9	1.4	0.3	–35.9	87.55	0.0031	92/065.7–069.1	3.4	4.5	1.65
107	92/098.7	2.5	0.5	–35.9	85.22	0.0010	92/090.8–095.4	4.7	6.7	2.08
108	92/126.2	2.3	0.7	–35.9	83.32	0.0025	92/119.0–122.1	3.1	6.1	0.99
109	92/155.3	4.5	0.9	–35.1	81.32	0.0028	92/144.1–150.7 ^c	6.5	8.9	2.96
110	92/247.0	9.0	1.6	–35.8	75.66	0.0015	92/226.2–234.1 ^a	7.9	16.3	3.00
111	92/292.2	4.3	2.0	–35.7	72.54	0.0058	92/279.7–285.4	5.8	10.4	3.52
201	02/332.5	2.9	3.4	44.0	–36.39	0.0341	02/324.4–325.8	1.4	6.7	1.15
202	03/192.0	6.6	1.8	58.0	–48.28	0.0383	03/176.0–184.4 ^c	8.4	12.7	3.76
203	03/238.1	5.5	1.5	64.0	–46.20	0.0073	03/226.9–235.0 ^c	8.1	8.5	3.95
204	03/263.6	1.8	1.4	67.0	–42.01	0.0024	03/257.9–261.9	4.0	4.8	2.38
205	03/288.3	7.5	1.2	72.0	–33.58	0.0056	03/276.0–286.3	10.3	8.5	2.67
206	03/315.7	1.2	1.1	76.0	–10.30	0.0169	03/310.7–314.1	3.4	4.4	4.22
207	03/337.5	2.7	0.9	76.0	22.82	0.0258	03/333.5–336.0	2.5	2.6	3.80
208	03/364.5	3.0	0.9	70.0	56.91	0.0011	03/360.5–364.2	3.7	2.5	4.49
209	04/025.6	4.1	0.8	57.0	71.68	0.0042	04/019.9–024.6	4.7	3.7	5.24
210	04/050.0	3.7	0.8	44.0	77.82	0.0017	04/045.6–049.9	4.3	2.6	2.88
211	04/080.2	8.1	0.9	29.0	81.20	0.0009	04/074.3–082.1	7.8	1.8	2.58
212	04/155.3	10.0	1.2	3.0	82.07	0.0443	04/150.6–155.0	4.4	0.3	2.46
213	04/169.7	12.0	1.3	0.0	81.68	0.1385	04/161.3–166.1	4.8	2.4	1.44
214	04/181.0	10.0	1.4	–2.0	81.32	0.0640	04/174.5–179.1	4.6	1.5	2.08
215	04/190.2	2.4	1.5	–4.0	80.99	0.0028	04/187.8–192.2	4.4	1.2	1.92
216	04/202.0	3.0	1.5	–5.0	80.53	0.0038	04/199.0–201.9	2.9	1.5	2.87
217	04/215.8	6.9	1.6	–7.0	79.94	0.0039	04/203.4–207.2 ^b	3.8	8.9	0.78
218	04/231.0	6.0	1.8	–9.0	79.13	0.0013	04/225.9–229.1	3.2	2.1	2.21
219	04/246.0	4.0	1.8	–11.0	78.46	0.0024	04/234.5–241.0	6.5	9.5	3.04
220	04/302.5	5.0	2.2	–16.0	75.35	0.0058	04/286.5–290.8	4.3	13.5	1.48
221	04/331.8	1.0	2.4	–18.0	73.62	0.0068	04/323.8–325.6	1.8	7.5	0.81
222	04/362.3	1.2	2.6	–19.0	71.71	0.0051	04/354.2–355.5	1.3	7.5	2.64
223	05/044.2	5.0	3.0	–21.0	68.53	0.0089	05/027.8–033.0	5.2	13.9	5.34
224	05/082.6	3.9	3.2	–23.0	66.97	0.0045	05/071.7–075.9	4.2	9.0	3.08
225	05/123.9	2.0	3.5	–24.0	63.11	0.0088	05/120.8–125.4	4.6	2.1	2.97
226	05/175.3	3.0	3.8	–25.0	59.44	0.0222	05/169.6–172.2 ^b	2.6	4.2	2.88
227	05/209.8	3.0	4.0	–26.0	56.93	0.0475	05/192.7–194.4	1.7	15.6	2.60
228	05/228.6	4.0	4.1	–26.0	55.44	0.1462	05/214.2–217.4	3.2	12.4	6.95

^a Very close and successive CIRs separated by few days that are considered as a single event.

^b It is not clear whether it is a CIR or a Coronal Mass Ejection (CME) or both.

^c CIR preceded by a CME considered as a single event.

regions where plasma is compressed and leads to a stronger deflection of interplanetary dust grains trajectories provided by either CIRs or the leading regions of CMEs. For simplicity, we will usually refer to either of these events simply as compression regions (CRs), bearing in mind that in the majority of cases these are CIRs.

A direct comparison between the Jovian dust streams and the IMF and solar wind data from both Ulysses' Jupiter flybys (Fig. 1) shows that every dust stream is preceded by at least one CR. This fact can easily be observed in Fig. 1a–m where every dust stream (bottom panel, numbered shaded rectangles) and its associated compression regions (vertical dark gray stripes) are highlighted. Of course with CIRs occurring on average every two weeks, there is always a CR shortly (few days) before a dust stream, though sometimes at the same time. These former CRs are precisely the ones that are highlighted with darker tones, since they likely influence the dust streams. Our next task is to determine whether these associations are random or have a direct cause and relationship with the dust streams.

Notice that in Fig. 1 and for the time periods that we consider for our study, when possible, all CRs are highlighted with gray

stripes. Darker stripes represent the CRs that are likely associated to dust streams chosen as the immediate preceding CR, either a CIR or a CME.

We introduce Fig. 4 as a complement of Fig. 1, in order to have a better comparison of both flybys and to highlight some features that play an important role in our analysis and that are discussed in the following sections. The top panel shows the joviocentric detection distances of each stream during both flybys (+: first flyby and Δ : second flyby). The middle panel shows the dust flux of each dust stream. Note in this panel a *peak* (212–214) in the flux (second flyby) that corresponds to the Jovian equatorial plane crossing. The bottom panel shows the time separation between each dust stream and its precedent compression region, which show a variation with distance.

3.2. Dust stream durations

Fig. 1a–m and Table 1 suggest that the duration of dust streams (Δt_s) is well connected to the duration of the CRs (Δt_c). The average impact rate of most interplanetary and interstellar particles detected by the dust detector in quiet times is around

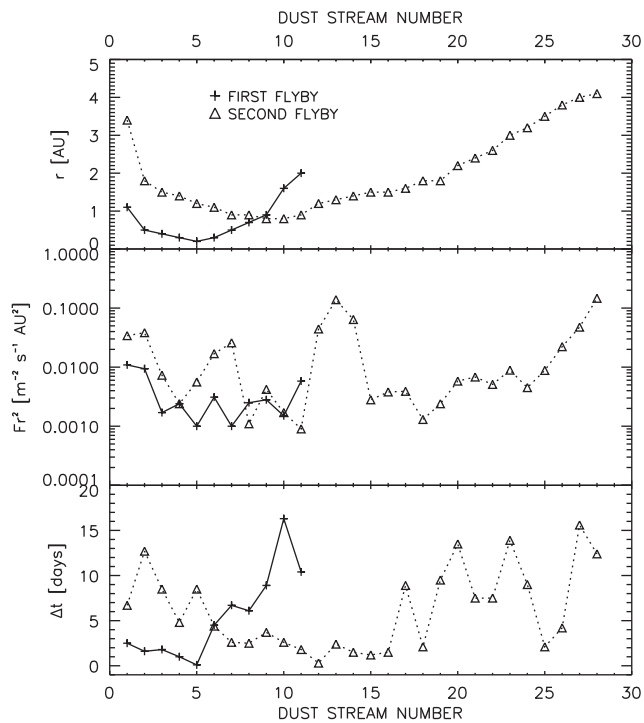


Fig. 4. Comparison of the joviocentric distance (top), the dust stream flux (middle) and CR-dust stream offset for both flybys. Plus symbols and continuous lines represent the first flyby and triangles and dotted lines represent the second flyby.

one impact every 10 days. The dust stream flux can increase this rate by one to four orders of magnitude. These enhancements define how long or short dust streams are. We refer the reader to Baguhl et al. (1993) and Krüger et al. (2006b) for the dust stream duration calculation details. The dust streams durations determined this way are listed in Table 1, column 3 with accuracies of approximately ± 0.5 days.

For comparison purposes, we also calculate the durations of CIRs and/or CMEs. Since CIRs are bounded by forward and reverse shocks it is somewhat easier to get their durations more accurately. By contrast, the durations of CMEs, and indeed their identification, is more uncertain since these are bounded – in the most evident cases – only by a fast forward shock. Nevertheless we only consider the duration of the compression region that leads the CME, which in most cases can be inferred with the aid of the other properties of the solar wind – like density and temperature – and the IMF.

Note that in some cases, complicated CRs are correlated with dust streams of similar complex appearance. An excellent example is stream 211 which, although classified as a single stream of 8.1 day duration in Table 1, has a double-peaked structure and may in fact be two streams separated by few days (Fig. 1h, days 74–84). Interestingly, two CIRs occur just prior to the two streams. As Ulysses was about 30° above the Jovian equator at this point, strong positive forces (note the F_n trace) were required to deflect grain trajectories upward; and indeed, strong positive F_n values occur 1–2 days before each sub-stream. A more borderline example is dust stream 205 (Fig. 1g), which has a long duration but might also possibly be better separated into two distinct streams. This stream follows two chained CIRs between days 276.0 and 286.3. Clearly in most cases CIR and stream identification are a bit subjective. For analysis purposes in this paper, we consider all of these possible double events as long single events.

Also note that streams 211 and 205, with durations of around 7 days, are almost twice as long as the average stream duration. In fact, streams 212, 213 and 214 are even longer, showing durations

of about 10 days (Fig. 1i). There is not an obvious way to separate these streams into several smaller ones and, conversely, a case can be made for combining streams 213 and 214 and perhaps even 212 into one continuous and extremely long dust stream! Strong and regular CIRs also occur during this time, but their durations do not correlate with the durations of the dust streams. There is clearly another effect at work here. Most likely, the fact that Ulysses was near the Jovian equator during this time period is important, as dust trajectories do not need to be altered as much and, thus have a higher chance to reach the dust sensor. This would naturally lead to a higher flux. These long streams are, nevertheless, indicated for reference purposes in the summary figures we will present below.

Fig. 5 shows the direct comparison of the dust stream durations and the durations of their previous CR. We have used the dust stream numbers as markers to highlight the individual durations. Both, the durations of dust streams and their precedent CRs are similar, typically around 4 days. Both flybys are analyzed separately as well considering that, in each case, the dust stream detection geometry was different, which seems to make a difference as can be seen comparing Fig. 5a and b. Even though the durations are well correlated, the correlation coefficients confirm this dependence on geometry: The first flyby data shows a better correlation coefficient (0.80) than the second flyby (0.69). For our statistical purposes, we note that streams 212, 213 and 214 were atypically long and we exclude them from our correlation analysis. In the following sections we will also keep this separate analysis of both flybys.

3.3. CRs and dust stream non-simultaneous detection

In Section 3.1, we have shown that the dust streams appear shifted in time with respect to the precedent high IMF event. It is also evident that the closer to Jupiter, the closer in time also the occurrence of every dust stream with respect to its previous event. Thus, this time delay between the detection of a CR and the detection of the dust stream that follows varies with the distance from Ulysses to Jupiter. For analysis purposes this offset is measured from the beginning of each dust stream to the beginning of the precedent IMF event. This correlation is shown in Fig. 6. Fig. 6a shows that the correlation coefficient in the first flyby data set is 0.78. The second flyby data (Fig. 6b) shows a weaker correlation coefficient (0.54) in particular, due to the dust streams detected farther away from Jupiter. Still, in a good number of cases, we can say that the delay between each stream and its precedent CR grows with the joviocentric distance.

The traveled distance depends on the traveling speed of the grains through interplanetary space and, in turn, this speed depends on the acceleration mechanisms inside the Jovian magnetosphere. This problem has been discussed by many authors over the past 15 years (Horányi et al., 1993, 2000; Hamilton and Burns, 1993; Flandes, 2004). Considering that Zook et al. (1996) estimated grain velocities (≥ 200 km s $^{-1}$) and that Horányi et al. (1993) derived values between 300 and 400 km s $^{-1}$, we adopt $v \sim 400$ km s $^{-1}$ and we can say that dust grains traverse the Jovian magnetosphere in about 3 h and, afterwards, travel an AU in about 4 days. For all dust streams, therefore, the dust travel time is well approximated by the interplanetary portion of its trajectory, i.e. t_s (days) $\approx 4.3r$ (AU).

3.4. Dust stream intensities

The intensity of each dust stream seems to depend on the intensity of its precedent CR, suggesting again that dust streams are, at least, modulated by the CRs. In fact, intense (roughly $B \geq 2$ nT) and/or long CRs lead to intense and/or long dust streams, and weak CRs lead to weak streams or no stream at all.

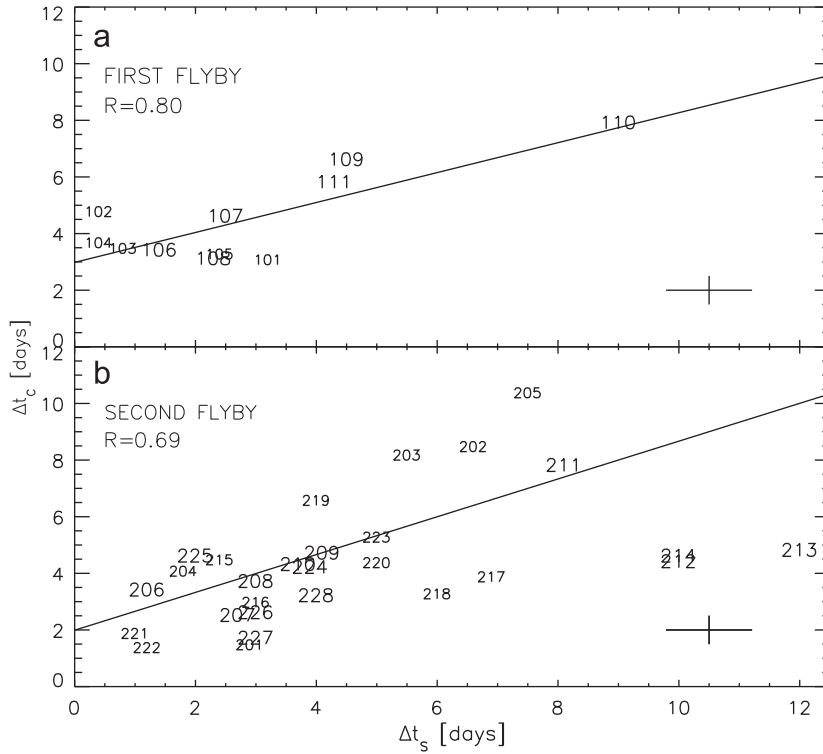


Fig. 5. Least squares trend of the durations of the high IMF events (Δt_c) and the dust streams (Δt_s) during both Ulysses Jupiter flybys. The duration of each dust stream seems to be a consequence of the duration of CRs. We use the stream numbers as markers for a better analysis. The smaller number size of the markers indicates $\beta < 0$. Typical error bars are shown at the bottom right of the figure. R stands for the correlation coefficient of the fit in each case. We highlight that due to their atypically long durations, streams 212, 213 and 214 were not considered in the correlation, but they are shown for comparison.

Weak CRs likely produce dust streams only near the Jovian magnetosphere and the Jovian equatorial plane where the dust population is larger. Examples of this can be seen throughout the full data set as in Fig. 1h, where a couple of weak CIRs (one, $B \sim 1.4$ nT, around day 10 in 2004 and the other, $B \sim 1.5$ nT, around day 30, both close to Jupiter, but with the spacecraft at high latitude $\beta > 50^\circ$) do not produce dust streams. However, there are some cases when no dust streams are detected even after strong enough CRs. Take for example Fig. 1a, between days 290 and 330 in 1991. Even though there is a faint hint of streams in the dust rate profile, there are not enough dust impacts for a clear stream identification. A probable explanation to this lies in the fact that the dust flux from Jupiter, though continuous, is not steady at all. Two main factors are involved in this. One is the dust production through Io's volcanism and the other is the plasma environment in Jupiter's magnetosphere. The first one controls the dust supply into the plasma torus and the magnetosphere; the other controls the dust charging and therefore the Jovian dust supply to the interplanetary medium. Nevertheless, a comparison between the dust stream flux and their precedent CR's magnetic field intensity apparently show contradictory results (see Fig. 7). The first flyby data supports the former hypothesis and shows a clear correlation ($R=0.75$) between both sets. In contrast, the second flyby data does not show an apparent correlation. Again distance and geometry may explain this discrepancy.

4. Interaction of dust streams with the IMF

4.1. Grain charge

During the grains' journey away from Jupiter, their surface electric charge Q is not strictly constant. In particular, inside the

plasma torus, the different plasma conditions modulate Q . Higher dusk side temperatures result in dominance of secondary electron emission currents over the other currents producing positively charged dust grains that will be able to escape from the Jovian magnetosphere (Horányi et al., 1997). These grains have typical $\phi \approx +5$ V surface potentials (equivalent to ≈ 35 fundamental charges if $a=10$ nm). Outside of the magnetosphere, Q could be affected essentially by the interaction with the solar wind ions and electrons and the UV solar radiation. The effects of the UV photons on the dust stream grains can be evaluated with

$$I_v = 2.5 \times 10^{10} \pi a^2 e (\chi / r_{AU}^2) \exp(-e\phi/kT_v) \quad (1)$$

which approximates the production of photoelectrons due to solar UV radiation from positively charged dust grains (Horányi et al., 1988). Here χ is the efficiency factor whose value can be taken as 0.1 for dielectric conductors such as silicates. If at $r_{AU} = 5.2$, the UV photons' energy is of the order of $kT_v \approx 2$ eV, the electron current from a 10 nm particle would be 0.001 electrons/day which is a very low rate for the periods of time considered in our study. In general, collection currents from solar wind ions and electrons are more efficient than UV photoemission currents.

Solar wind charging effects are more efficient than UV photons'. The solar wind is mainly characterized by ions and electrons. Solar wind ions have an average energy of the order of 1 keV at the orbit of Jupiter and electrons around 1 eV, nevertheless the dust stream grains have velocities that are comparable to the solar wind particles, therefore, in some cases, collisions may involve larger energies. On average, the grain net charging will depend on the initial sign of its charge, its relative velocity with respect to the ions/electrons and the encounter frequency between grains and solar wind particles. This frequency of encounters may tell us how relevant these encounters are for charging purposes. Let us define this rate as $T = v\lambda^{-1}$ with v as the

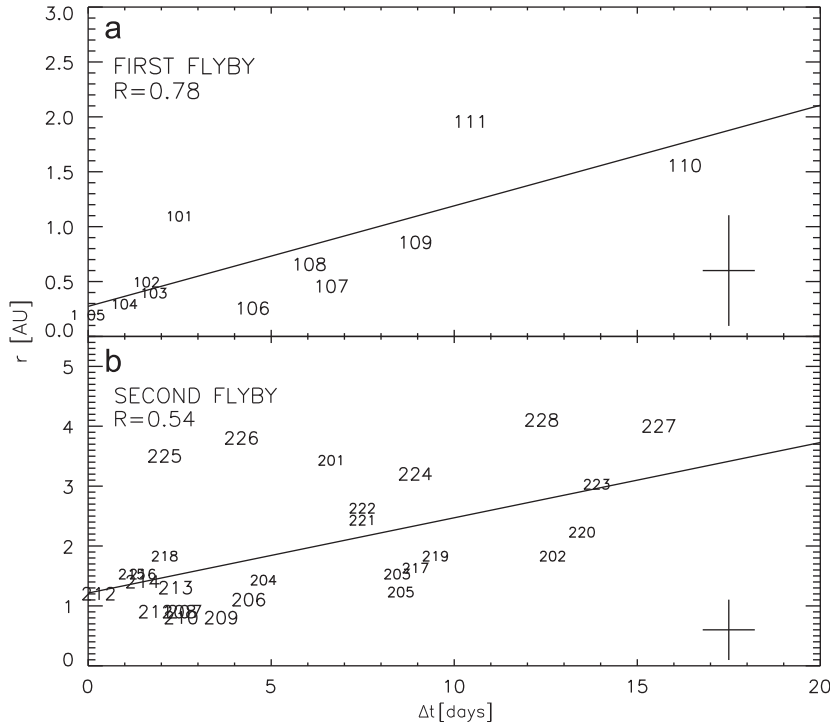


Fig. 6. Least squares trend of the dust stream detection distance r from Jupiter versus the time delay Δt between the beginning of the precedent high IMF events and the beginning of the most probable dust stream from the 1991–1992 to 2002–2005 Ulysses data set. Smaller symbols indicate $\beta < 0$. Typical error bars are shown at the bottom right of the figure. The correlation coefficient R is given in each case.

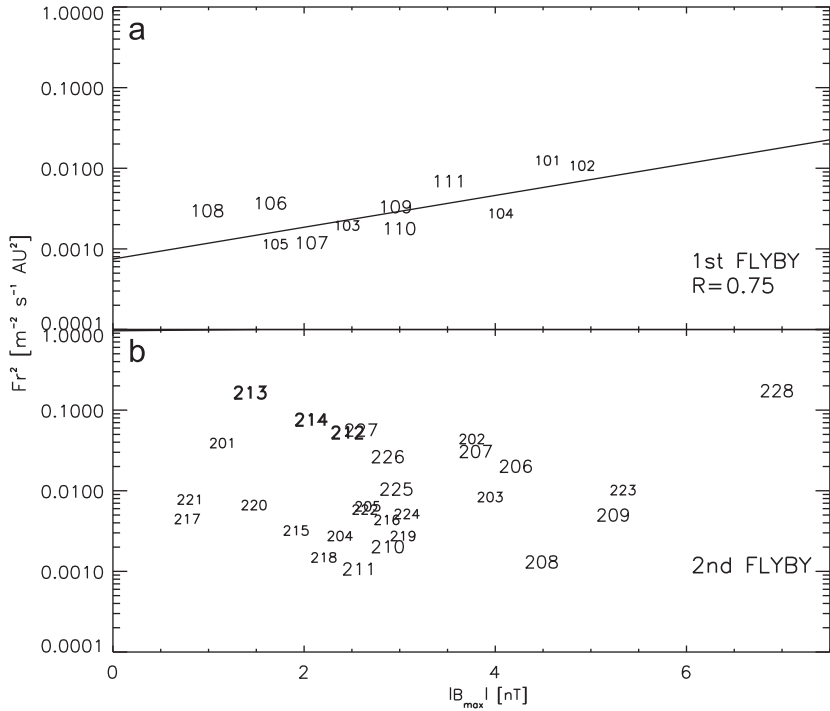


Fig. 7. Dust stream flux versus maximum magnetic field intensity of the precedent event. The dust flux has been multiplied by the square of the distance to Jupiter to correct for the varying spacecraft distance from Jupiter. The top plot (first flyby) shows a least squares fit trend that indicates a correlation, nevertheless, the second flyby (bottom plot) shows no correlation.

velocity of the dust grains with respect to the solar wind and λ the mean free path, which is defined in terms of the solar wind ion/electron density n and σ is the capture cross-sectional area of the dust grains, i.e. $\lambda = (n\sigma)^{-1}$. The rate is then

$$T = n\sigma v \tag{2}$$

As in Dyson and Williams(1997), by conservation of energy and angular momentum, we assume

$$\sigma = \pi a^2 [1 \pm 2Ze^2 / (4\pi\epsilon_0 a m_i u_i^2)] \tag{3}$$

Ze (> 0 , in this case) represents the charge of the grain and u_i is the velocity of the incident particles. We use the *plus* sign if

electrons and *minus* if ions. Even though most of the bulk mass of the solar wind is due to the ions, from the Ulysses data, we know that the solar ion density and the total number density of electrons per cubic centimeter are similar as well as the ion and the total electron temperatures. The solar wind plasma moves as an ensemble of particles and therefore we can also assume the same speed for both species. Combining Eqs. (2) and (3) we have that the maximum number of ion encounters ($\sim 7.43 \text{ day}^{-1}$) is slightly less than the maximum number of electron encounters ($\sim 7.50 \text{ day}^{-1}$). Ions and electrons may be captured by the grains, but some of these encounters may also produce loss of material on the grains by sputtering electrons if the collisions are sufficiently energetic. Furthermore, if we only assume capture of ions/electrons, the change rate of ϕ would also be *small* such that a typical grain would require more than 2 months (≈ 79 days) to change its ϕ by 1 V (seven charges). On the other hand, a simple capture of ions and electrons seems to turn grains more negative, but since a fraction of these ions/electrons would produce electron emission, this excess of negative charge could be compensated by positive charges, and in the long run, grains could turn slightly more positive considering the contribution of photo-ionization as well. According to Postberg et al. (2006), dust streams grains' composition is mainly NaCl, but sulphur or sulphurous components may be another constituent in the grains. A minor fraction also shows silicon components which implies that the gossamer ring cannot be ruled out as a minor source ($\sim 5\%$) of the stream particles. As reference, we know that for SO_x grains, incident electrons with optimum energies around 300 eV have yields around 3 (Horányi et al., 1997). Both, the small sizes of dust stream particles and the low number densities of the solar wind within a few AU of Jupiter greatly slow the rate that dust grain acquires electric charges. Accordingly, dust grain charges may be considered nearly constant during the grains' approximately week-long journeys to the spacecraft.

4.2. Grain motion

Grains that escape from Jupiter, depart from positions near or at the Jovian equatorial plane, but since the Jovian magnetic field axis is tilted 10° w.r.t. the planet's rotation axis, grains will not necessarily follow escape trajectories along or close to the Jovian equatorial plane. However, though the magnetic axis may keep a constant tilt w.r.t. the rotation axis and the ecliptic plane, its relative inclination w.r.t. the Sun varies as Jupiter moves about it. This implies that, at least, for the Jovian grains that Ulysses detected inside Jupiter's orbit and that escape toward the Sun or near the Sunward direction, the inclination of their escape trajectories w.r.t. the ecliptic plane may depend on the position of the planet along its orbit. For these grains, the inclinations of their escape trajectories from the magnetosphere are likely within a $\sim 20^\circ$ interval centered at the ecliptic. Data shows (Fig. 3b) that the number of detected dust streams increased when the spacecraft was not only near the planet but close to the ecliptic plane. Nevertheless, dust streams were also detected at medium and high jovigraphic latitudes and these large detection angles suggest that the dust grains' motion is largely deflected from their original ejection direction while they travel through the interplanetary space.

A simple and satisfactory first explanation of the dust stream production, which we complement with actual data in this section, was published by Hamilton and Burns (1993). These authors assumed that the motion of the charged dust grains ejected from the magnetosphere of Jupiter is only perturbed along the direction perpendicular to the ecliptic plane. This theoretical model states that an alternate periodic perturbation due to the IMF variation connected with the solar rotation leads to a periodic

upward and downward oscillation in the dust particles' trajectories perpendicular to the ecliptic plane. The largest deflections occur when grains undergo the influence of the enhanced IMF of CIRs and CMEs and thus, stronger CRs lead to stronger deflections.

The influence of the IMF on the charged dust grains not only depends on the IMF strength (see Fig. 6) but also on the solar wind speed. Furthermore, it also strongly depends on the direction of motion of the grains with respect to this field. This direction is defined by the departing position of the grains around Jupiter when they escape from the Jovian magnetosphere, expressed by the jovigraphic longitude L .

The grains move along increasing spiral trajectories around Jupiter inside the Jovian magnetosphere (Grün et al., 1998). Due to conservation of angular momentum, the tangential component of their velocity declines as the radial component grows while the grains move away from Jupiter. It drops to quite small values at the limits of the magnetosphere. Thus we can assume that the grain departing longitude is held fairly constant outside the magnetosphere.

Ahead we describe the interaction of a test dust grain with the IMF in terms of Jovian geometric parameters as well as solar wind parameters in the vicinity of Jupiter. We start with the electromagnetic force as driving force (in MKS):

$$\mathbf{F} = Q\mathbf{v}' \times \mathbf{B} \quad (4)$$

where \mathbf{B} is the IMF vector essentially represented by its tangential component $B_{t_{\text{IMF}}}$ and \mathbf{v}' is the relative velocity of the dust grains with respect to the IMF. c ($= 2.99 \times 10^8 \text{ m s}^{-1}$) is the speed of light. The relative velocity of the grains depends on their velocity v with respect to Jupiter and the velocity of the solar wind V as well as on the longitude L . Again, the radial velocity of grains can be assumed constant since only weak forces act on the grains along the radial direction and the magnitude of \mathbf{v}' can be defined as follows:

$$v' = V + v \cos L \quad (5)$$

According to the assumptions made, the magnitude of Eq. (4) is

$$F = Qv'B_{t_{\text{IMF}}} \quad (6)$$

Note that this force is calculated from the data and it is displayed in the sixth panel of Fig. 1a–m (in arbitrary units), thus giving a better idea of the deflection direction. Grains feel a stronger force under the influence of a compression region and a less intense force under average IMF conditions. The polarity of the solar magnetic field defines whether particles are deviated upwards or downwards with respect to the ecliptic plane. From Eq. (6) the upward/downward acceleration is given by

$$\alpha = \left(\frac{\phi}{\pi \rho k a^2} \right) v' B_{t_{\text{IMF}}} = 0.132 v' B_{t_{\text{IMF}}} \quad (7)$$

where $k = 8.987 \times 10^9 \text{ N m}^2 \text{ C}^2$. We have assumed the same typical spherical dust particle values as in Eqs. (2) and (3). For the sake of simplicity, in the second member of this former equation, the units of the magnetic field were adjusted to nanoteslas and the speed's units to hundreds of kilometers. Since, under our general assumption, the force is perpendicular to the direction of motion, we can assume, following Hamilton and Burns (1993), that dust particles, whose average motion is along the ecliptic plane, recede from the ecliptic plane in sections of parabolic trajectories. Unlike Hamilton and Burns (1993), who assumed significantly larger grains with far slower speeds, here one segment of a parabola usually suffices. Accordingly, the vertical position z of a grain can be described by

$$z = \pm \frac{1}{2} \alpha t^2 = \pm 0.066 v' B_{t_{\text{IMF}}} t^2 \quad (8)$$

Since the distance traveled by dust in the ecliptic plane is simply vt , we can easily obtain the jovigraphic latitude as a function of time:

$$\beta = \pm \tan^{-1} \left[0.0666 B_{\text{IMF}} \left(\frac{V + v \cos L}{v} \right) t \right] \quad (9)$$

Eq. (9) summarizes the relationships between the physical properties that play important roles in the production and dynamics of dust streams. It also makes some interesting predictions that we might see in the data. The most important point is that β is a function of L , the angle between the Sun and the dust trajectory projected into the ecliptic; if $V \approx v$, it is a strong function of L . Thus, all else being equal, dust streams can be expected to be deflected more strongly out of the ecliptic plane when they are directed toward the Sun ($L=0$). Under average IMF conditions, i.e. $B_{\text{IMF}} \approx 0.5$ nT, with a single polarity, dust grains can gain a latitude $\beta \approx \pm 7^\circ$ in only 2 days; this is increased to $\beta \approx \pm 25^\circ$ if, while escaping, the grains encounter an average CIR with its enhanced B_{IMF} .

The dust particles that escape along the Jupiter–Sun line ($L=0^\circ$) are the fastest in the frame of reference of the moving IMF and therefore the effects of this field will be the greatest with respect to other grains ejected in different directions. It is tempting to argue, therefore, that CIRs have a greater effect for dust streams projected toward the Sun, however, this is not so. The time that a dust stream remains in a CIR of given radial length r_{CIR} is simply $t = r_{\text{CIR}} / (V + v \cos L)$ which, when inserted into Eq. (9), cancels out the longitude dependence. Sunwardly projected dust streams experience stronger deflection forces but for a shorter amount of time. In this case, the detector geometry, which is not considered here, probably plays a major role (Krüger et al., 2006a).

In any case, these effects will be greater inside the compression regions than under average IMF conditions. In particular, for the dust grains ejected from the day side of the magnetosphere, the relative perpendicular velocity will be maximum when $L=0^\circ$ ($v' = 2v_{\text{sw}}$) and minimum when $L=90^\circ$.

The grains ejected from the night side of the magnetosphere are another interesting case, since their perpendicular velocity with respect to the IMF is, on average, much smaller than on the day side. In particular, near $L \sim 180^\circ$ the perpendicular velocity is very small and at $L = 180^\circ$ it nearly vanishes because $v \approx V$. Thus, grains are only slightly affected by the IMF, receding from Jupiter along nearly straight-line trajectories.

5. Conclusions

In this work we have done a direct comparison of the Ulysses solar wind, IMF and dust data in order to have a better picture of how the motion of the dust grains ejected by Jupiter is modulated to produce the Jovian dust streams. This demonstrates how relevant the periodic intensity variations of the solar wind and the IMF are in this modulation. We highlight some important and evident features from the data:

First, there is always a previous high IMF event associated with an observed dust stream. These events are, in most cases, corotating interaction regions, and in a few cases, Coronal Mass Ejections (Fig. 1).

Second, the duration of each dust stream roughly matches the duration of a precedent CR (Fig. 5).

Third, the occurrence of each dust stream and the occurrence of the previous CR are separated by a time interval that depends on the distance to the planet (Fig. 6).

Fourth, the intensity of the compression regions (CRs) is connected to the intensities of the successive dust streams such

that intense events produce intense streams and weak events produce weak dust streams or no dust streams at all (Fig. 7). This holds at least in the case of the first flyby data. There is no such correlation in the second flyby, indicating the importance of detector geometry.

Out of these facts, we can conclude that strong enough CRs are key in the detection of the so-called Jovian dust streams, which are an enhancement in the local dust density observed by the spacecraft. Evidence seems to indicate that CIRs and CMEs, through strong vertical deflections, modify this local dust density. Furthermore, enhancements in the dust flux seem to occur when the heliospheric current sheet sweeps across the spacecraft. Depending on the polarity of the interplanetary magnetic field, which varies with the solar cycle, dust may be attracted to or repelled from the current sheet. The complicated interplay between CRs, and the current sheet – as well as the dust detector's pointing geometry – likely can account for the fact that some strong CRs are not followed by streams. Furthermore, some small dust streams may not have been noticed in the dust data; here we have confined our analysis to the dust streams identified by Baguhl et al. (1993) and Krüger et al. (2006b) that account for those streams that have the highest probability of occurrence. However, notice that other possible weak and short dust streams can be seen in the data (e.g. Fig. 1a: day 329, Fig. 1b: days 57–60, Fig. 1d: days 264–267 and Fig. 1h: days 57 and 101).

The distance from the source and geometry seems to play a quite important role as can be seen in the correlations shown in Figs. 5–7. On the one hand, the first flyby data, where the detection was closer to Jupiter, show acceptable coefficients, while in the case of the second flyby, the correlations decrease. A possible explanation is that the longer the grains travel away from Jupiter, the more coupled with the IMF the grains will be. If true, it is probable that in the long run a good portion of the grains that compose the dust streams would be eventually dragged by the IMF.

Of course, there are other variables that affect Jovian dust stream properties, such as the volcanic activity of Io, the plasma density in the torus or the general plasma conditions around Jupiter. For example, surface changes on Io give evidence of not only a continuous, but also a variable volcanic activity (Geissler et al., 2004) that modulates the amount of material – dust included – that is transported away from the satellite. On the other hand, asymmetries in the temperature profile in the plasma torus may also vary the charging conditions, affecting the dust flux which is ejected to the interplanetary medium (Horányi et al., 1997).

Finally, we conclude that the dynamical effects on the Jovian dust streams we have investigated here mainly apply within a few astronomical units from Jupiter such that dust grains flight times are short. A description of the long term effects of the solar wind will be a subject of a future work. Our investigation of the Jovian dust streams will be applicable to the saturnian dust streams as well, since the same physical mechanisms are at work at Saturn. Furthermore, dust streams should also form at the other giant planets Uranus and Neptune, provided that a sufficiently strong dust source exists. This study may also stimulate new investigations of the dust-magnetosphere interaction within the Jovian magnetosphere as measured with Galileo. We also hope that the data shown in Fig. 1 will be useful for further studies of the dust stream formation mechanisms.

Acknowledgments

Part of this work was carried out at the Jet Propulsion Laboratory under contract with NASA. Part of this work was also carried out at the Max-Planck-Institut für Sonnensystemforschung in Katlenburg-Lindau during a research stay. The authors thank

Reiner Schwenn for his support in the CIRs and CMEs identification. A. Flandes thanks D. Maravilla and her support through the project DGAPA IN111207. The authors thank A. Graps and S. Kempf for thorough reviews.

References

- Baguhl, M., Grün, E., Linkert, G., Siddique, N., 1993. Identification of small dust impacts in the Ulysses dust detector data. *Planetary and Space Science* 41, 1085–1098.
- Balogh, A., Beek, T.J., Forsyth, R.J., Hedgecock, P.C., Marquedant, R.J., Smith, E.J., Southwood, D.J., Tsurutani, B., 1992. The magnetic field investigation on the Ulysses mission: instrumentation and preliminary scientific results. *Astronomy and Astrophysics Supplement Series* 92, 221–236.
- Bame, S., McComas, D., Barraclough, B., Phillips, J., Sofaly, K., Chavez, J., Goldstein, B., Sakurai, R., 1992. The Ulysses solar wind plasma experiment. *Astronomy and Astrophysics Supplement Series* 92, 237–265.
- Dyson, J.E., Williams, D.A., 1997. *The Physics of the Interstellar Medium (The Graduate Series in Astronomy)*. second ed. Institute of Physics Publishing, Bristol, Philadelphia.
- Flandes, A., 2004. Dust escape from Io. *Geophysical Research Letters* 31 (16) CiteID 16802.
- Flandes, A., Krüger, H., 2007. Solar wind modulation of Jupiter dust stream detection. In: Krüger, H., Graps, A. (Eds.), *Workshop on Dust in Planetary Systems (ESA SP-643)*, September 26–30, 2005, Kauai, Hawaii, pp. 87–90.
- Geissler, P., McEwen, A., Phillips, C., Keszthelyi, L., Spencer, J., 2004. Surface changes on Io during the Galileo mission. *Icarus* 169 (1), 29–64.
- Grün, E., Krüger, H., Graps, A.L., Hamilton, D.P., Heck, A., Linkert, G., Zook, H.A., Dermott, S., Fechtig, H., Gustafson, B.A., Hanner, M.S., Horny, M., Kissel, J., Lindblad, B.A., Linkert, D., Mann, I., McDonnell, J.A.M., Polansky, G.E.M.C., Schwehm, G., Srama, R., 1998. Galileo observes electromagnetically coupled dust in the Jovian magnetosphere. *Journal of Geophysical Research* 103 (E9), 20011–20022.
- Grün, E., Zook, H.A., Baguhl, M., Bame, A.B.S.J., Fechtig, H., Forsyth, R., Hanner, M.S., Horanyi, M., Kissel, J., Lindblad, B.A., Linkert, D., Linkert, G., Mann, I., McDonnell, J.A.M., Morfill, G.E., Phillips, J.L., Polansky, C., Schwehm, G., Siddique, N., Staubach, P., Svestka, J., Taylor, A., 1993. Discovery of Jovian dust streams and interstellar grains by the Ulysses spacecraft. *Nature* 362 (6419), 428–430 (ISSN 0028-0836).
- Hamilton, D.P., Burns, J.A., 1993. Ejection of dust from Jupiter's Gossamer ring. *Nature* 364 (6439), 695–699 (ISSN 0028-0836).
- Horányi, M., Grün, E., Heck, A., 1997. Modelling the Galileo dust measurements at Jupiter. *Geophysical Research Letters* 24, 2175–2178.
- Horányi, M., Houpis, H.L.F., Mendis, D.A., 1988. Charged dust in the Earth's magnetosphere. I. Physical and dynamical processes. *Astrophysics and Space Science* 144 (1–2), 215–229 (ISSN 0004-640X).
- Horányi, M., Morfill, G., Grün, E., 1993. Mechanism for the acceleration and ejection of dust grains from Jupiter's magnetosphere. *Nature* 363 (6425), 144–146 (ISSN 0028-0836).
- Horányi, M., Morfill, G., Grün, E., 2000. Dust streams from Jupiter and Saturn. *Physics of Plasmas* 1 (10), 3847–3850.
- Hsu, H.W., Kempf, S., Jackman, C.M., 2010. Observation of saturnian stream particles in the interplanetary space. *Icarus* 206 (2), 653–661.
- Jones, G.H., Arridge, C.S., Coates, A.J., Lewis, G.R., Kanani, S., Wellbrock, A., Young, D.T., Cray, F.J., Tokar, R.L., Wilson, R.J., Hill, T.W., Johnson, R.E., Mitchell, D.G., Schmidt, J., Kempf, S., Beckmann, U., Russell, C.T., Jia, Y.D., Dougherty, M.K., Waite, J.H., Magee, B.A., 2009. Fine jet structure of electrically charged grains in Enceladus' plume. *Geophysical Research Letters* 36 (16) CiteID L16204.
- Kempf, S., Srama, R., Postberg, F., Burton, M., Green, S.F., Helfert, S., Hillier, J.K., McBride, N., McDonnell, J.A.M., Moragas-Klostermeyer, G., 2005a. Composition of saturnian stream particles. *Science* 307 (5713), 1274–1276.
- Kempf, S., Srama, R., Postberg, F., Horányi, M., Burton, M., Helfert, S., Moragas-Klostermeyer, G., Roy, M., Grün, E., 2005b. High-velocity streams of dust originating from Saturn. *Nature* 433 (7023), 289–291.
- Krieger, A.S., Timothy, A.F., Roelof, E.C., 1973. A coronal hole and its identification as the source of high velocity solar wind stream. *Solar Physics* 29, 505–525.
- Krüger, H., Altabelli, N., Anweiler, B., Dermott, S.F., Dikarev, V., Graps, A.L., Grün, E., Gustafson, B.A., Hamilton, D.P., Hanner, M.S., Horányi, M., Kissel, J., Landgraf, M., Lindblad, B.A., Linkert, D., Mann, I., McDonnell, J.A.M., Morfill, G.E., Polansky, C., Schwehm, G., Srama, R., Zook, H.A., 2006a. Five years of Ulysses dust data: 2000–2004. *Planetary and Space Science* 54 (9–10), 932–956.
- Krüger, H., Dikarev, V., Anweiler, B., Dermott, S.F., Graps, A.L., Grün, E., Gustafson, B.A., Hamilton, D.P., Hanner, M.S., Horányi, M., Kissel, J., Linkert, D., Linkert, G., Mann, I., McDonnell, J.A.M., Morfill, G.E., Polansky, C., Schwehm, G.H., Srama, R., 2010. Three years of Ulysses dust data: 2005 to 2007. *Planetary and Space Science* 58, 951–964.
- Krüger, H., Geissler, P., Horányi, M., Graps, A.L., Kempf, S., Srama, R., Moragas-Klostermeyer, G., Moissl, R., Johnson, T.V., Grün, E., 2003. Jovian dust streams: probes of the Io plasma torus. *Geophysical Research Letters* 30 (2), 30–31 CiteID 1058, doi: 10.1029/2002GL015920.
- Krüger, H., Graps, A.L., Hamilton, D.P., Flandes, A., Forsyth, R.J., Horányi, M., Grün, E., 2006b. Ulysses Jovian latitude scan of high-velocity dust streams originating from the Jovian system. *Planetary and Space Science* 54 (9–10), 919–931.
- Maravilla, D., Flandes, A., 2005. Possible sources for the saturnian dust streams. *Geophysical Research Letters* 32 (6) CiteID L06202.
- Oberst, J., Nakamura, Y., 1991. A search for clustering among the meteoroid impacts detected by the apollo lunar seismic network. *Icarus* 91, 315–325.
- Postberg, F., Kempf, S., Srama, R., Green, S.F., Hillier, J.K., McBride, N., Grün, E., 2006. Composition of Jovian dust stream particles. *Icarus* 183, 122–134.
- Zook, H.A., Grün, E., Baguhl, M., Hamilton, D.P., Linkert, G., Liou, J.C., Forsyth, R., Phillips, J.L., 1996. Solar wind magnetic field bending of Jovian dust trajectories. *Science* 274, 1501–1503.